Original article

Sol Roselli, Cecilia Deyá*, Mariana Revuelta, Alejandro R. Di Sarli and Roberto Romagnoli

Zeolites as reservoirs for Ce(III) as passivating ions in anticorrosion paints

https://doi.org/10.1515/corrrev-2017-0090
Received August 1, 2017; accepted December 8, 2017

Abstract: The aim of this paper was to evaluate the performance of two different modified zeolitic minerals as anticorrosion pigments in order to reduce or eliminate zinc phosphate in paints. In the first stage, the selected minerals were characterized and modified with cerium ions to obtain the anticorrosion pigments. Their inhibitive properties were evaluated by means of electrochemical techniques (corrosion potential measurements and polarization curves) employing a steel electrode immersed in the pigments suspensions. In the second stage, solvent-borne paints, with 30% by volume of the anticorrosion pigment, with respect of the total pigment content, were formulated. The performance of the resulting paints was assessed by accelerated (salt spray and humidity chambers) and electrochemical tests (corrosion potential measurements and electrochemical impedance spectroscopy) and compared with that of a control paint with 30% by volume of zinc phosphate. Results obtained in this research suggested that zeolites can be used as carriers for passivating ions in the manufacture of anticorrosion paints with at least reduced zinc phosphate content.

Keywords: coatings; corrosion; electrochemical impedance spectroscopy; zeolitic minerals.

1 Introduction

Organic coatings are widely used in metal protection because they constitute a physical barrier to water, ions, and oxygen. They can also provide additional protection by means of anticorrosion pigments – traditionally, chromates and lead compounds. These compounds are banned or about to be banned in some countries due to their harmful effect on human health (Klaassen, 1999; Gottesfeld, 2015). Zinc phosphate (PZ) and related substances became the leading substitutes for traditional toxic inhibitors commonly employed in paints. Three generations of phosphates were introduced in the market, PZ being the precursor (Gerhard & Bittner, 1986; Bittner, 1989; Romagnoli & Vetere, 1995a; Lenz et al., 2007; Yan et al., 2009; Hao et al., 2013) and modified zinc phosphates and different polyphosphates, the following (Meyer, 1963; Barraclough & Harrison, 1965; Szklarska-Smialowska et al., 1969; Fragata & Dopico, 1991; Romagnoli & Vetere, 1995a,b; Jaškova & Kalendová, 2012; Naderi & Attar, 2009; Naderi et al., 2013; Xiangyu et al., 2013; Bhanvase et al., 2014). However, these compounds based on phosphate anions and heavy metals, particularly zinc and strontium, are being questioned by their negative impact on the environment, which is why new replacements are being proposed. Phosphate ion causes eutrofication of water reservoirs, whereas heavy metals are toxic for humans and/or animals (Odum, 1972; Klaassen, 1999).

More recently, the challenge in the field of paint technology is to formulate smart coatings for providing an optimum selective response to some external stimulus, for instance, corrosion. Ideally, a smart corrosion protective coating will generate or release an inhibitor only when demanded by the onset of corrosion (Baghdachi, 2004; Zarras & Stenger-Smith, 2015). These coatings are based on multi-functional micro- and/or nanocontainers, which are incorporated into polymer or hybrid coating matrixes for active anticorrosion protection. A nanocontainer (or nanoreservoir) is a nanosized volume filled with an active substance confined in a porous core and/or shell, which precludes the direct contact between the active agent and the adjacent environment. In smart coatings, the inhibitor release is triggered by some external stimulus: pH, aggressive ions, etc. This type of inhibitor often provides a multi-level self-healing approach by combining damage prevention and restoration mechanisms within the same system. These mechanisms may include the entrapment

***Corresponding author: Cecilia Deyá,** Centro de Investigación y Desarrollo en Tecnología de Pinturas (CIDEPINT), CICPBA-CONICET, Av. 52 s/n e/121 y 122, B1900AYB, La Plata, Argentina, e-mail: c.deya@cidepint.gov.ar
Sol Roselli, Mariana Revuelta, Alejandro R. Di Sarli and Roberto Romagnoli: Centro de Investigación y Desarrollo en Tecnología de Pinturas (CIDEPINT), CICPBA-CONICET, Av. 52 s/n e/121 y 122, B1900AYB, La Plata, Argentina

of corrosive ions, corrosion inhibition, and water displacement from active defects, etc. (Shchukin & Möhwald, 2007; Zheludkevich et al., 2012).

One of the most common reservoirs is the group of nanocrystalline layered double hydroxides (LDHs), which are able to store and release inhibitive anions like vanadates, molybdates, etc. (Zheludkevich et al., 2010; Tedim et al., 2011; Hang et al., 2012; Montemor et al., 2012; Yuhua et al., 2013; Carneiro et al., 2015; Shkirskiy et al., 2015; Yan et al., 2016). Intelligent anticorrosion coatings based on pH-responsive nanocontainers that release entrapped corrosion inhibitor were developed, employing hollow silica nanoparticles. Silica nanoparticles may be covered alternatively layer-by-layer with polyelectrolyte layers and layers of inhibitor (Zheludkevich et al., 2007; Ávila-Gonzalez et al., 2011; Chen & Fu, 2012; Borisova et al., 2013; Zarras & Stenger-Smith, 2015). Ceramic nanocontainers were also developed for entrapping corrosion inhibitors (Kartsonakis et al., 2012; Lakshmi et al., 2017).

Self-healing microcapsules were designed to improve the efficiency of anticorrosion paints in cases of abrasion and scratching. Microcapsules are currently filled with film-forming materials and corrosion inhibitors (Szabó et al., 2011; Eunjoo et al., 2014).

Some natural occurring minerals could be useful as micro- and/or nanoreservoirs for inhibitive species and were employed to formulate anticorrosion coatings. In this sense, the use of bentonite and halloysites has been reported. Calcium bentonite is a cation exchange pigment (Granizo et al., 2011). Halloysites are naturally occurring tubular containers for different organic corrosion inhibitors (Abdullayev et al., 2009; Liu et al., 2009; Falcón et al., 2015; Feng & Cheng, 2016). Except for calcium bentonite, the other containers were allowed to formulate paints with similar performance to those containing chromates.

Zeolites are also microcontainers of the hydrated aluminosilicates of the alkaline and alkaline earth metals group. Their structures have Si-O-Al linkages that form surface pores of uniform diameter and enclose regular cavities and channels of discrete sizes and shapes, which depend on the chemical composition and crystal structure of the specific zeolite being considered (Zalba, 1996).

These physicochemical characteristics of zeolites determine two important properties of these compounds: the possibility of water sorption and that of cation exchange, both in a reversible way and without causing changes in their structure (Zalba, 1996). This last property makes them useful for a wide number of industrial applications such as ion exchangers, dietary supplements in animal husbandry, reforming petroleum catalysis, puzzolanic materials for cements and concrete, etc. (Ming & Allen, 1997; Armbruster, 2001).

In spite of the extensive diversification of the uses of zeolites in the last half century, their application to paints is still poorly developed. They have been incorporated into different coatings with different purposes: as humidity adsorbers, to avoid secondary reactions that would occur in the presence of humidity and polyuretanic resins (Ferrazzini, 1986), to retain the antimicrobial properties of a biocide (Ming & Allen, 1997); and as extender pigments (Torii, 1978; Columbié Pineda et al., 1991). Zeolite microparticles were also used as reservoirs for Ce(III) in sol-gel coatings and for molybdenum cations in anticorrosion coatings (Dias et al., 2012; Deyá et al., 2013).

It is well known that many cations, which form insoluble hydroxides (Greenwood & Earnshaw, 1984), may be employed as cathodic inhibitors; this applies particularly to rare earths cations (Behrsing et al., 2014). Lanthanides have low toxicity, and their ingestion or inhalation has not been considered harmful to humans (Haley, 1965); toxic effects of their oxides are similar to those produced by sodium chloride (DHHS-NIOSH, 1986). Furthermore, lanthanides can be considered as economically competitive products because some of them are relatively abundant in nature. The relative abundance of cerium, for instance, is similar to that of copper. The production of lanthanides has increased continuously in recent years. Lanthanides, principally cerium, have found to have many different applications in corrosion protection at high temperatures (Lu & Ives, 1993), to improve the adherence of oxide films of different metallic alloys by ionic implantation, etc. (Bethencourt et al., 1998; Zhu et al., 2013).

The purpose of this study was to prepare cerium-modified zeolites to formulate anticorrosion paints in which phosphates could be partially or totally replaced. The modified zeolites were prepared by ionic exchange, and their anticorrosion properties, assessed by electrochemical techniques. Afterwards, coatings were formulated and, their performance was evaluated by accelerated (humidity and salt spray chambers) and electrochemical tests [corrosion potential, electrochemical impedance spectroscopy (EIS)]. Results showed that the exchanged zeolites could replace zinc phosphate in anticorrosion paints.

2 Materials and methods

The experimental section describes the two main activities of this research: (1) the preparation and assessment of the inhibitive properties of Ce(III) exchanged zeolites in solution and (2) the assessment of the inhibitive properties

of Ce(III) exchanged zeolites in anticorrosion paints. The electrochemical characterization of Ce(III) exchanged zeolites is mandatory because if an anticorrosion pigment fails to protect steel in solution, it must not be employed to formulate paints (Deyá et al., 2010). Finally, it must be incorporated into paint formulation just to assess its performance in the presence of the paint components.

2.1 Preparation and characterization of cerium-exchanged zeolites

2.1.1 Minerals characterization

Two different samples of zeolitic rocks were used in this research. Their qualitative mineralogical composition was obtained by X-ray diffraction (XRD) once the rock was ground. After grinding, the minerals morphology was examined by scanning electron microscopy (SEM) and their surface composition was obtained by energy dispersive X-ray analysis (EDX). The ground natural minerals density was determined by pycnometric method according to ASTM G 153 standard specification. Zinc phosphate (PZ) powder was also observed by SEM, and its elemental composition, obtained by EDX. A FEI Quanta 200-s microscope and a RX microanalyzer with the EDX detector Apollo 40 were employed.

Two zeolites minerals were tested, and, for the sake of clarity, from now on, the two minerals will be referred to as Z1 and Z2 (Table 1).

2.1.2 Preparation of cerium-exchanged zeolites

The zeolitic rocks were ground to obtain fine-grain powder whose average particle size was <10 μm. After being ground and washed twice with distilled water (DW), they were placed for 1 h in a beaker with boiling 0.2 M HNO_3 to solubilize ferric compounds. The acid solution was added from time to time to keep the solution volume constant. The solids were separated from the supernatant by centrifugation at 2200×*g* for 10 min and washed with DW several times. Then, they were placed in a beaker with 2 M $NaCH_3COO$ for 3 h under continuous stirring to put the zeolite back into the Na form. Afterwards, the ground minerals were separated by centrifugation and washed twice with DW. Finally, they were exchanged with Ce(III) ions by bringing them into contact for 24 h with a 1 M $Ce(NO_3)_3$ under constant stirring. At last, the exchanged minerals were separated by centrifugation, washed four times with DW, and dried in an oven at 90°C until constant weight. From now on, the exchanged zeolites will be labeled as ZCe.

A scheme of this procedure is presented in Figure 1.

Table 1: Nomenclature of the tested anticorrosion pigments.

Nomenclature	Meaning
Z	Zeolite
Z1	Zeolite 1 (mordenite)
Z2	Zeolite 2 (mordenite and heulandite)
PZ	Zinc phosphate
ZNa	Zeolite exchanged with sodium
ZCe	Zeolite exchanged with cerium
Z1Ce	Zeolite 1 exchanged with cerium
Z2Ce	Zeolite 2 exchanged with cerium
ZCe + PZ	Zeolite exchanged with cerium + zinc phosphate
Z1Ce + PZ	Zeolite 1 exchanged with cerium + zinc phosphate
Z2Ce + PZ	Zeolite 2 exchanged with cerium + zinc phosphate

2.1.3 Cation exchange capacity

In order to determine the minerals capability of being a reservoir for the passivating ions, the cation exchange capacity of the zeolites was measured. In this sense, sodium exchange capacity and that for cerium ions were determined for both zeolites.

The ground mineral was put into contact for 3 h with 2 M $NaCH_3COO$ under continuous stirring. Then, the sorbed sodium was back extracted into solution with 100 ml of 1 M NH_4CH_3COO, per each gram of the corresponding mineral, by continuous stirring during 24 h. The solid was then separated by centrifugation, and Na ions were quantified in the supernatant by atomic absorption spectroscopy.

In order to determine the cerium exchange capacity of the zeolitic minerals, the sorbed ion was back extracted into solution with 100 ml of 1 M NH_4CH_3COO, from 1 g of the corresponding modified zeolites by continuous stirring for 24 h. The solid was then separated by centrifugation, and Ce was quantified in the supernatant by a gravimetric technique (Welcher, 1948). A 70-ml aliquot of the solution containing Ce(III) was acidified with 10 ml of 2 M acetic acid and treated with a slight excess of 3% weight/volume (w/v) 8-hydroxyquinoline (C_9H_7NO) in ethyl alcohol. Cerium "oxinate", $Ce(C_9H_6ON)_3$, was then precipitated by adding 20 ml of 10% w/v ammonium hydroxide and heating the solution to boiling point. The purple-brown precipitate was separated by centrifugation at 2200×*g* for 5 min, washed with hot water, dried at 110°C, and weighed in an analytical balance (precision 0.1 mg). The cerium exchanged per gram of zeolite may be calculated from the amount of precipitated (W_{solid}) by the following equation:

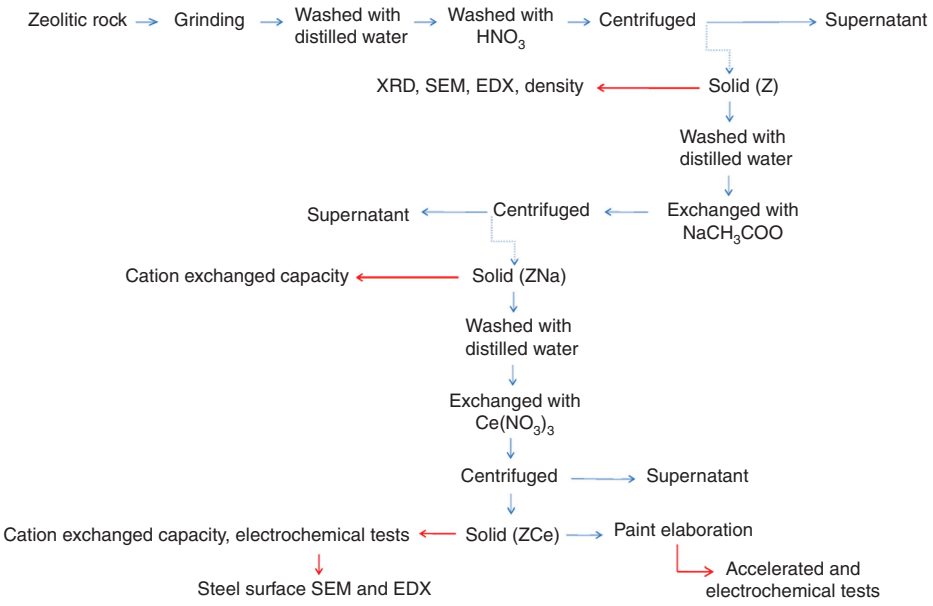

Figure 1: Scheme of the exchanged-zeolites preparation and testing.

$$\text{Percentage of cerium (\%)} = \frac{24.5 * W_{\text{solid}}}{1\,\text{g}}$$

The control was a cerium solution containing 0.1 g of Ce(III) in 70 ml. In every case, determinations were done in triplicate.

2.1.4 Electrochemical tests

The protective behavior of Ce(III) was assessed by electrochemical techniques. The corrosion potential (Ecorr) evolution of commercial SAE 1010 steel electrodes, immersed in Ce(III) solutions, was measured as a function of time, with respect to the saturated calomel electrode (SCE) as reference. The cerium nitrate concentration varied from 1.15×10^{-5} to 4.6×10^{-4} M. These solutions were employed to simulate the Ce(III) concentration leached from the exchanged zeolites in the supporting electrolyte (NaCl 0.025 M). For the sake of comparison, Ecorr of steel immersed in 0.025 M NaCl was also measured. Measurements were performed during 4 h and in duplicate. The same measurements were carried out using a suspension of the anticorrosion pigments.

Linear polarization tests were also done, employing the Ce(III) solutions whose concentration varied from 1.15×10^{-5} to 4.6×10^{-4} M. The SCE was used as reference, and a platinum grid, as the counter electrode. Measurements were done after 2 and 4 h of immersion. Polarization resistance (Rp) and corrosion rate (Icorr) were calculated from these curves. The swept amplitude was ±20 mV from the open circuit potential, and the scan rate, 0.166 mV · s^{-1}. The exposed area was 0.28 cm^2. Measurements were carried out with the 273A EG&G PAR Potentiostat/Galvanostat in combination with model SOFTCORR 352 software (EG&G PAR). The same measurements were carried out using suspensions of the anticorrosion pigments. Values were compared with the Rp and Ic obtained for PZ and a control solution (without inhibitor).

The inhibitive efficiency (E) was calculated with the equation

$$\text{E} = \frac{I_0 - I}{I_0} \times 100$$

I_0 = Icorr for the blank; I = Icorr for the tested specimen.

Potentiodynamic scans were done, employing 0.5 M NaCl, SCE as reference and a platinum grid as the counter electrode and SAE 1010 steel as working electrode. Three different suspensions were tested: one containing zeolite 1 exchanged with cerium ions (Z1Ce), another containing cerium-exchanged zeolite 2 (Z2Ce), and the third one containing zinc phosphate. The swept amplitude was ±250 mV from the open circuit potential, and the scan rate was 0.2 mV · s^{-1}. The exposed area was 0.28 cm^2. Measurements were performed after 2 h of immersion.

Measurements were carried out with the 273A EG&G PAR Potentiostat/Galvanostat in combination with model SOFTCORR 352 software (EG&G PAR).

In polarization measurements, the concentration of the supporting electrolyte was increased to improve both the cell conductivity and the Ce(III) exchange from the zeolite.

In Table 1, the nomenclature of the samples is shown, while in Table 2, a summary of the electrochemical tests is presented.

2.1.5 Observation and characterization of the exposed surface

Steel panels in contact with the cerium nitrate solutions, the suspensions of the exchanged zeolites (ZCe), and the mixtures ZCe + PZ were observed by SEM after Ecorr measurements were finished.

2.2 Formulation, elaboration, and application of paints

The binder used to prepare the paint films to carry out this research was a medium oil alkyd (52% sunflower seed oil). Paints formulation may be seen in Table 3. Paint 1A and paint 2A have only modified zeolite as anticorrosion pigment, while paints 1B and 2B contained zinc phosphate plus the modified minerals. The total anticorrosion pigment content, by volume, was the same for all the paints, 30%, referring to the total pigment content, which is the percentage recommended in the literature to achieve good results with phosphate pigments (Gerhard & Bittner, 1986; Romagnoli & Vetere, 1995a; del Amo et al., 1996; Romagnoli et al., 2000). Barium sulfate, titanium dioxide, and talc were incorporated to complete the pigment formulas. As control, a paint with the same PZ content (7.5% of PZ, referred to the total paint formula) was formulated.

The pigment volume concentration to the critical pigment volume concentration relationship (PVC/CPVC) was 0.8, as suggested in current literature for phosphate pigments (Gerhard & Bittner, 1986; Romagnoli & Vetere, 1995b; del Amo et al., 1996; Romagnoli et al., 2000). The CPVC value was determined by the oil absorption method according to ASTM D 1483 standard specification, and the PVC value was then obtained from the CPVC and the selected PVC/CPVC ratio. The resin volume (Vr) corresponding to pigment volume (Vp) was obtained considering that $PVC = Vp/(Vp + Vr)$.

Pigments were dispersed in the vehicle (resin and solvent) for 24 h employing a ball mill in order to achieve an acceptable dispersion degree (5 in Hegman's gage). Wetting and dispersant additives were added during paints preparation (1% of the total paint formulation each one). Substrate wetting and leveling additives were added before painting (0.45% each one). Cobalt and calcium drier were also added, 0.06% and 0.12%, respectively.

SAE 1010 steel panels ($15.0 \times 7.5 \times 0.2$ cm) were firstly sandblasted, degreased with toluene, and painted by brush up to a dry film thickness of 70 ± 5 μm. Finally, they were kept indoors for 14 days before testing.

Table 2: Details of the electrochemical tests carried out in this research.

	Tests
Cerium nitrate	
Corrosion potential	Electrolyte: NaCl 0.025 M Reference electrode: saturated calomel
Linear polarization curves	Electrolyte: NaCl 0.05 M Reference electrode: saturated calomel Counter electrode: Pt Swept amplitude: ±20 mV
Pigments	
Corrosion potential	Electrolyte: NaCl 0.025 M Reference electrode: saturated calomel
Linear polarization curves	Electrolyte: NaCl 0.05 M Reference electrode: saturated calomel Counter electrode: Pt Swept amplitude: ±20 mV
Potentiodynamic scans	Electrolyte: NaCl 0.5 M Reference electrode: saturated calomel Counter electrode: Pt Swept amplitude: ±250 mV
Paints	
Corrosion potential	Electrolyte: NaCl 0.5 M Reference electrode: saturated calomel
Electrochemical impedance spectroscopy	Electrolyte: NaCl 0.5 M Reference electrode: saturated calomel Counter electrode: Pt Frequency: 1×10^{-2}–1×10^{5} Hz

Table 3: Paints composition as percentage by volume.

Components	Paint				
	Control (C)	1A	1B	2A	2B
Zinc phosphate (PZ)	7.5	–	2.5	–	2.5
Zeolite 1 (Z1Ce)	–	7.5	5.0	–	–
Zeolite 2 (Z2Ce)	–	–	–	7.5	5.0
Barium sulfate	7.2	7.2	7.2	7.2	7.2
Titanium dioxide	2.9	2.9	2.9	2.9	2.9
Talc	7.2	7.2	7.2	7.2	7.2
Alkyd resin (1:1)	36.1	36.1	37.3	36.1	37.3
Solvent (white spirit)	39.1	39.1	37.9	39.1	37.9

2.3 Accelerated and electrochemical tests on painted panels

As the protection of the substrate is determined by a complex mechanism, accelerated tests in aging chambers and electrochemical tests to evaluate the performance of the formulated paints were carried out. A set of three panels was placed in the salt spray chamber (Atlas Model SF850, USA) according to ASTM B 117 standard specification. Another set of panels was placed in Sunvic type F102/3 humidity chamber (ASTM D 2247 standard). After 48, 192, 216, 312, and 500 h of exposure in the salt spray chamber, the rusting degree (ASTM D 610) was evaluated. As well, after 24, 72, and 168 h of exposure in the humidity chamber, the blistering degree (ASTM D 714) was also evaluated.

The corrosion potential (Ecorr) value of painted steel provides useful thermodynamic information about the passivity of the surface. Therefore, this magnitude was measured using electrochemical cells obtained by fixing an acrylic tube, 2-cm diameter, on the painted specimen and filling it with 0.5 M NaCl. The Ecorr of painted panels was measured with a high impedance voltmeter and using SCE as reference.

The anticorrosion performance of the specimens was also assessed by EIS in a three-electrode cell. Measurements were made with a Solartron 1250 frequency response analyzer. The frequency was varied between 1×10^{-2} and 1×10^{5} Hz. The counter and reference electrodes were a platinum mesh and SCE, respectively. The working electrode was the coated metal with an exposed area of 16 cm^2; 0.5 M NaCl was used as electrolyte. The highest NaCl concentration employed in this test was justified by the relatively high barrier effect of the alkyd system and allowed to obtain an adequate response in due time. Tests were done in duplicate.

A higher NaCl concentration was employed in the electrochemical tests on painted panels due to the insulating characteristics of the anticorrosion paint.

3 Results and discussion

3.1 Preparation and characterization of cerium-exchanged zeolites

3.1.1 Characterization and properties of the zeolitic minerals

The mineralogical composition of the zeolitic rocks obtained by XRD showed that Z1 contained a high proportion of mordenite $(Na_8)\{Al_8Si_{40}O_{96}\}\cdot 24H_2O$ (>80%), while Z2 presented a mixture of crystalline phases being mordenite (50–80%) and heulandite, $(Ca_4)\{Al_8Si_{28}O_{72}\}\cdot 24H_2O$ (30–50%), the major constituents. The natural minerals density was similar (Table 4).

SEM micrographs and EDX of both zeolites and zinc phosphate are shown in Figure 2. In every case, the particle size was <10 μm. This feature is important as the size of the pigments should be <20 μm to obtain a uniform dry paint film. The particle and particle size distribution of both zeolites did not differ significantly from those of PZ. The zeolitic minerals also contained iron compounds, which were eliminated by the nitric acid washing (del Amo et al., 2003).

The zeolites exchange capacity is shown in Table 4. The cation exchange capacity of both minerals towards Ce(III) was quite low and that of Z2 was four times higher than the capacity of Z1.

3.1.2 Electrochemical tests

At the beginning of the test period, no significant differences in steel Ecorr could be observed between the tested Ce(III) solutions, but after 50 min, differences became perceivable. The Ecorr of SAE 1010 steel immersed in Ce(III) solutions was displaced to values more positive than the blank. The shift towards more positive values depended on the Ce(III) concentration – Ecorr of the steel electrode immersed in the most diluted solution being the one with the most positive values. At the end of the test, steel immersed in Ce(III) solutions had corrosion potential values around −450 mV, while the blank fluctuated around −620 mV (Figure 3). These results showed that steel was less active in the presence of Ce(III) salts and that increasing Ce(III) concentration did not lead necessarily to an increase in Ecorr. This was confirmed by the determination of Rp and Icorr (Table 5). Ce(III) reduced steel corrosion rate. The anticorrosion efficiency may be higher than 98.5%. Cecílio and co-workers reported that cerium nitrate is preferable to cerium chloride because nitrate anion possess certain protective action (Cecílio et al., 2007).

In pigment suspensions, at the beginning of the exposure period, Ecorr was displaced to more positive values and dropped off as time elapsed (Figure 4). At the end of the immersion time, the steel Ecorr value was the most negative one and corresponded to steel undergoing corrosion. Instead, the steel Ecorr values in pigment suspension were at least 100 mV more positive because some kind of protection was achieved. Differences among the

Table 4: Properties of the zeolitic minerals.

Zeolite minerals	Mineral composition	Density (g/ml)	Cation exchange capacity (CEC)	
			meq Na^+/g mineral	meq Ce^{3+}/g mineral
Z1	Mordenite	2.11	0.73 ± 0.02	0.010 ± 0.001
Z2	Mordenite and heulandite	2.12	0.96 ± 0.02	0.040 ± 0.001

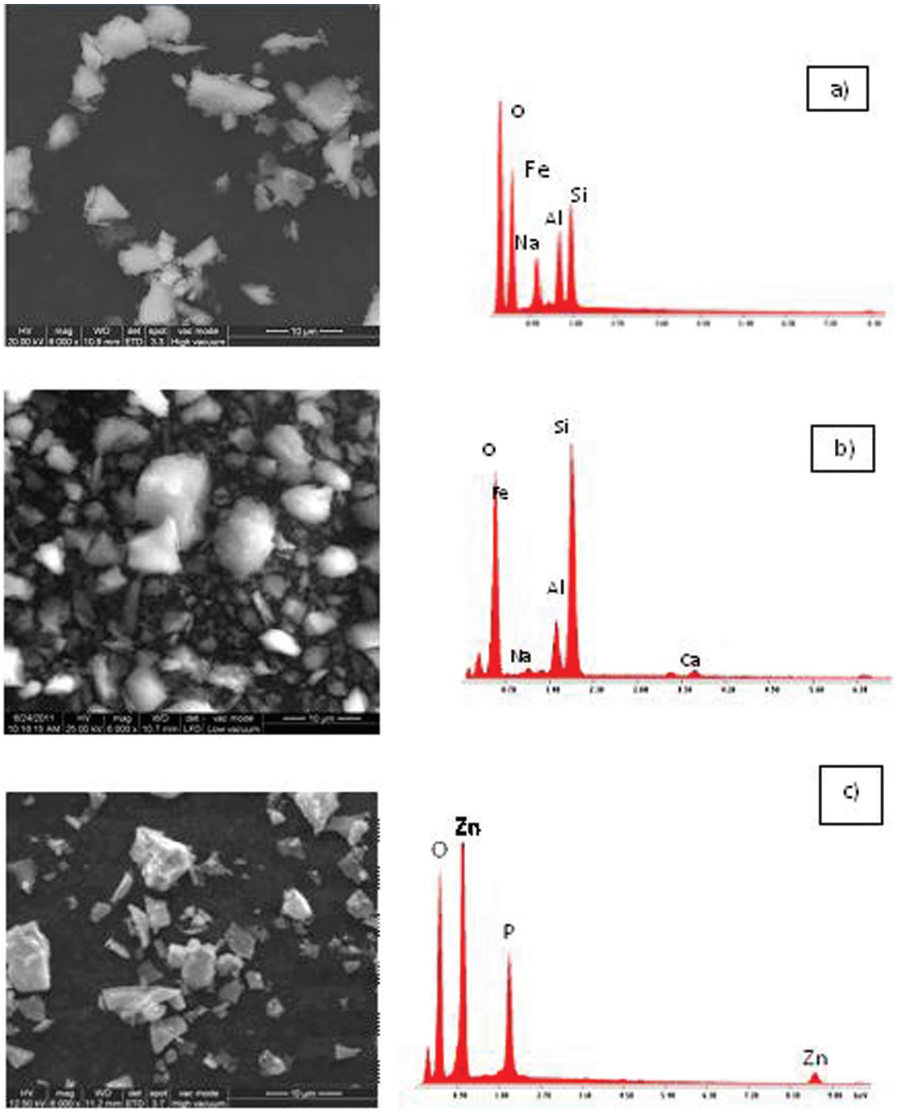

Figure 2: SEM micrographs (6000×) and EDX analysis of (A) zeolite 1, (B) zeolite 2, and (C) zinc phosphate powder.

pigments mixtures were not significant (≤50 mV). The best inhibitive pigment mixture seemed to be ZCe + PZ.

Ic and Rp values of steel in the pigments suspensions (Z, ZCe, and ZCe + PZ) were reported in Table 6. All the inhibitive pigments diminished corrosion rates when compared to the blank. The zeolites, by themselves, reduced Icorr according to their exchange capacity. Steel in the mixtures zeolite + zinc phosphate exhibited lower Ic values. Moreover, these values were similar to those obtained when PZ was used alone, thus indicating that PZ was responsible for this further reduction in Icorr.

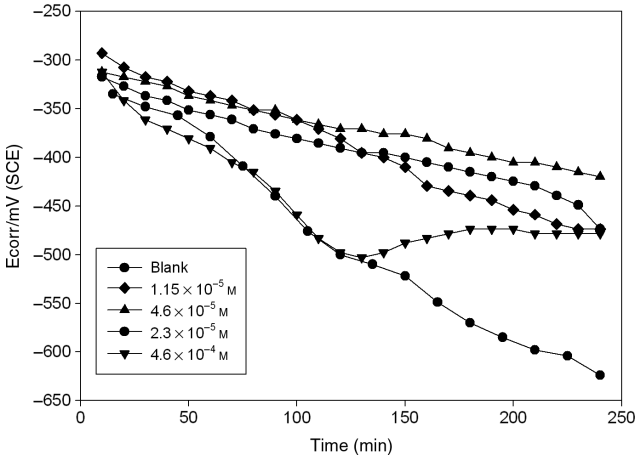

Figure 3: Corrosion potential of the samples immersed in 0.025 M NaCl at different concentrations of $Ce(NO_3)_3$.

The potentiodynamic scans showed that all the anticorrosion pigments diminished the anodic dissolution current in a similar way, with respect to the blank. Cathodic current was also diminished. These facts account for the inhibitive properties of the tested pigments (Figure 5).

3.1.3 Observation and characterization of the exposed surface

The morphology of the protective layer was observed by SEM; after 24 h of immersion in the above-mentioned solutions, steel was covered with a uniform film.

Globular oxides were observed for the lowest Ce(III) concentrations (Figure 6A), and the protective film presented a tendency to form pits, particularly at higher concentrations of Ce(III) (Figure 6B). Pits may be covered by corrosion products, which had a cerium content of 12.7%. Some stick-like formations had grown on the protective layer when the Ce(III) concentration was 4.6×10^{-5} M (Figure 6A). These sticks had 56.0% of Ce. The "over precipitation" of Ce-enriched particles has been reported elsewhere (Kesavan et al., 2012). Small amounts of Ce (2.5%) were also detected in certain globular formations (Figure 6B).

Figures 7–11 show the morphology of the protective coating formed on steel in contact with suspensions of PZ and of the exchanged zeolites (ZCe) or the mixture ZCe + PZ.

In the case of PZ, a homogeneous film was formed on the metal substrate, basically composed by iron oxyhydroxides, some agglomerations grown on it. These agglomerations were composed of P, Fe, and Zn, and it is thought that they plug the pores of the film (Figure 7A and B).

A homogeneous thin film was also observed in the case of Z1Ce (Figure 8A). At higher magnification (12,000×), corrosion products accumulations may be appreciated, which followed almost straight lines. These

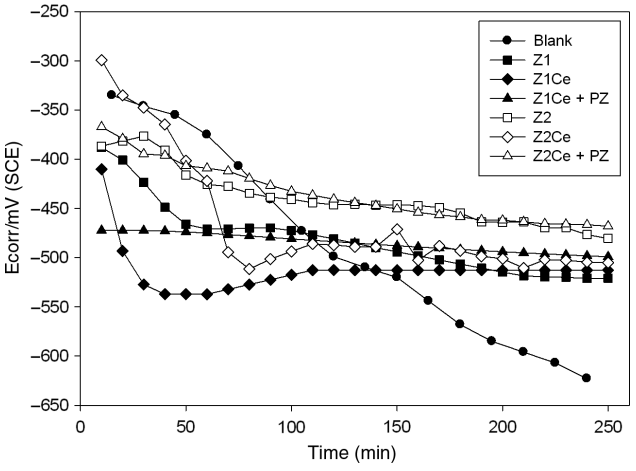

Figure 4: Corrosion potential of the samples immersed in 0.05 M NaCl with different anticorrosive pigment mixtures.

Table 6: Polarization resistance (Rp) and corrosion current (Ic) of SAE 1010 steel in pigments suspensions in 0.05 M NaCl after 2 h of immersion (PZ, zinc phosphate; Z1Ce, zeolite 1 exchanged with Ce; Z2Ce, zeolite 2 exchanged with Ce).

	Blank	Pigment suspensions				
		PZ	Z1Ce	Z1Ce+PZ	Z2Ce	Z2Ce+PZ
$Rp/k\Omega\cdot cm^2$	1.7	24.3	6.6	21.1	12.3	21.7
$Ic/\mu A\cdot cm^{-2}$	45.1	3.2	11.8	3.7	6.3	3.6

Table 5: Polarization resistance (Rp) and corrosion current (Ic) of SAE 1010 steel in $Ce(NO_3)_3$ solutions in 0.05 M NaCl after 2 h of immersion.

	Blank	$Ce(NO_3)_3$ concentration			
		4.6×10^{-5} M	1.1×10^{-4} M	2.3×10^{-4} M	4.6×10^{-4} M
$Rp/k\Omega\cdot cm^2$	1.0	22.9	30.03	9.6	41.7
$Ic/\mu A\cdot cm^{-2}$	84.2	1.2	1.6	2.6	3.0

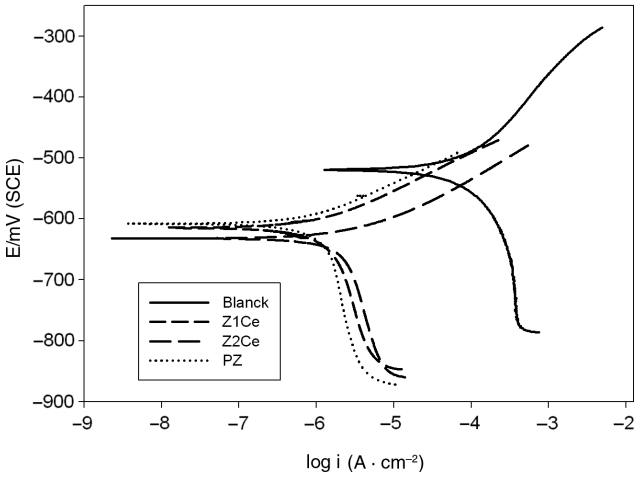

Figure 5: Potentiodynamic scans (Tafel mode) of the samples immersed in 0.5 M NaCl for 2 h with different anticorrosion pigments.

products contained small amounts of Ce (0.9%) (Figure 8B). As reported previously in the literature (Zhu et al., 2013), Ce(III) is incorporated in the oxide film, thus improving its protective ability. A low amount of zeolite was also incorporated in the protective film, as it could be deduced from the presence of Si (0.6%). The presence of Ce in the protective film was interpreted to come from an ionic exchange between the ZCe and cations like Na(I) associated to the aggressive chloride; this process may be represented by the following equation:

$$Ce^{3+}/3\,Z + 3\,Na^{1+} \leftrightarrow 3\,Na^{1+}/Z + Ce^{3+}$$

As ZCe was put in contact with the aggressive electrolyte NaCl, penetrating the coating, Ce(III) was released from the zeolite particle. Other cations will provoke the same exchange.

The film formed on steel exposed to the Z1Ce + PZ suspension was homogeneous (Figure 9A). According to EDX spectrum, it was composed mainly by iron oxyhydroxides, as Fe and O were detected. The protective film also contained small amounts of zeolite (0.19% of Si and 0.18% of Al) and phosphorus (0.33% of P). The incorporation of phosphate to the protective film was considered beneficial (Kozlowski & Flis, 1991). This base film appeared to be collapsed in some areas, exhibiting pits covered with corrosion products (Figure 9B). EDX analysis done inside these pits showed that the corrosion products contained P, Cl, Si, Fe, Al, and, in some cases, Zn (Figure 9B). The presence of P and Zn in the pits was supposed to favor pit repassivation as a consequence of their inhibitive properties. Some zeolite particles seemed to be deposited on the film (Figure 9C).

The protective film formed on steel in Z2Ce and Z2Ce + PZ suspensions presented similar morphologies. A more or less uniform film with a granule-like appearance was formed onto the metallic surface in contact with the Z2Ce suspension (Figure 10A and B). At higher magnification (12,000×), a cracked film was observed under these agglomerations (Figure 10B). The elemental analysis of these agglomerations revealed that they were mostly composed by silicon and cerium in a higher proportion than in the case of Z1Ce (Figure 10B). These agglomerations may be the Z2Ce particles depositing onto the metallic substrate. A greater amount of cerium (26%) was detected in the film underneath, which seemed to be constituted by iron oxyhydroxides (Figure 10B).

Cerium was not detected in the film formed on the steel in contact with the mixture Z2Ce + PZ, which was composed mainly of iron and oxygen (Figure 11A). Some pits appeared on the surface; several of them were covered by products with similar composition to the zeolitic mineral (Figure 11B). On the other hand, some pits were not covered, and the composition on the edge consisted of iron, sodium, silicon, zinc, and oxygen. Inside the pit, high content of iron was found, indicating that it may go all through the film (Figure 11C).

3.2 Accelerated and electrochemical tests on painted panels

3.2.1 Salt spray and humidity chambers

Results obtained in the salt spray chamber are shown in Table 7. According to the standard practice, the degree of rusting was evaluated using a 0–10 scale based on the percentage of visible surface rust. The rust distribution is classified as spot rust (S), general rust (G), pinpoint rust (P), or hybrid rust (H). Spot rust refers to rusting concentrated in a few localizes areas. General rust is concerned with rust spots of different sizes randomly distributed across the surface. Pinpoint rusted surfaces present rust distributed across the surface as very small individual specks.

Paint 2A, pigmented with Z2Ce, showed a disappointing protective behavior because it could not surpass 192 h of exposure. Corrosion spots appeared during the first week of testing; on the other hand, the other paints showed, at that moment, no rust. After 500 h of exposure, paints 1A and 2B had good qualification (rusting degrees 8P and 7G, respectively), while paint 1B was qualified with 5G, showing poorer protective performance. Paint 1 had the same anticorrosion behavior compared with

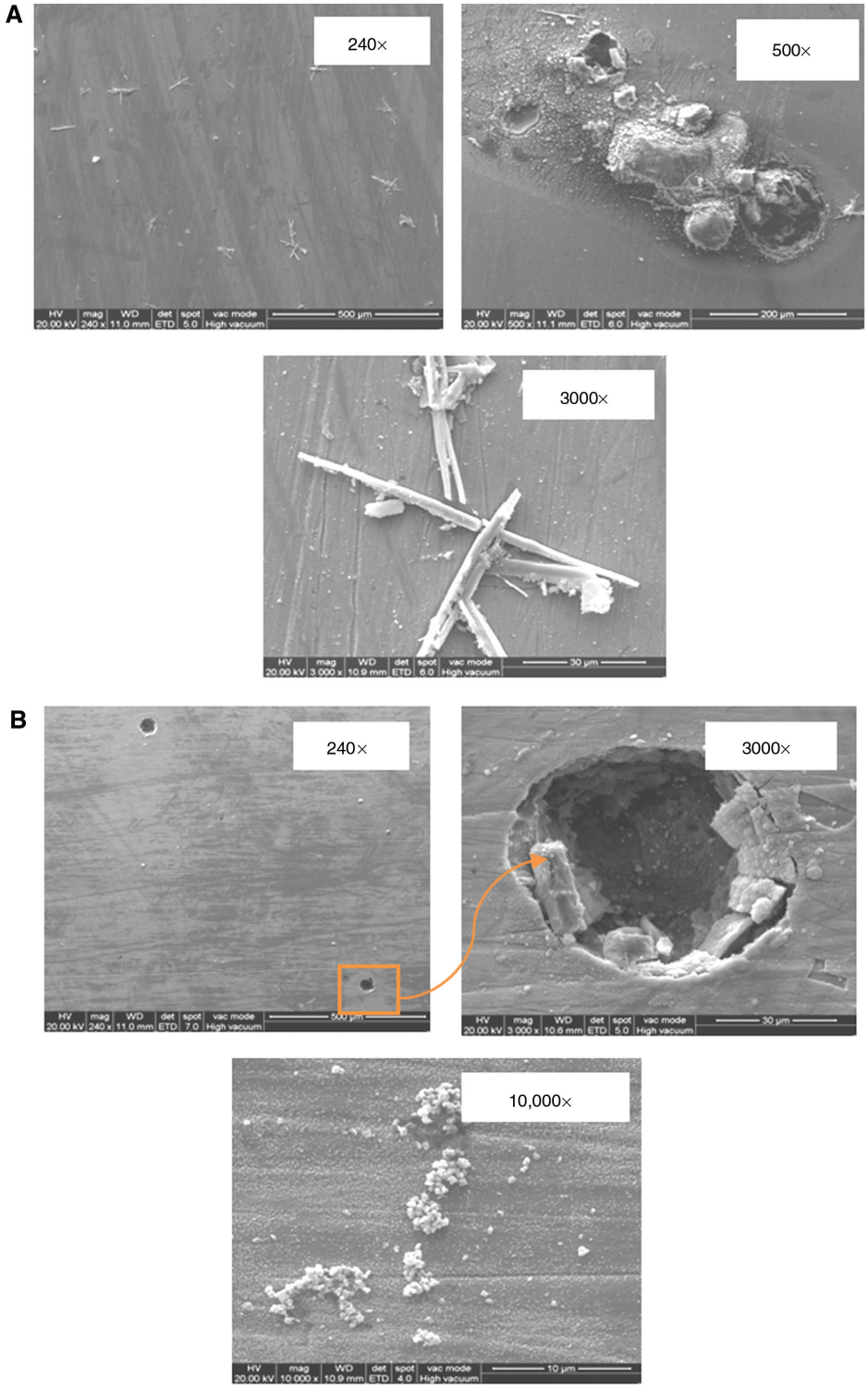

Figure 6: SEM micrograph of the protective film formed on the steel panels in contact with cerium (III) nitrate solution (A) 4.6×10^{-5} M and (B) 4.6×10^{-4} M in 0.025 M NaCl.

the control paint; so, it is possible to totally replace PZ by Z1Ce. The use of Z2Ce alone led to poorer performance, but in combination with a reduced amount of PZ, it led to acceptable results. The employment of modified zeolites allowed partial or full replacement of PZ, which depended on the selected zeolite.

The standard test method for evaluating the degree of paints blistering refers to the size and the density of blisters

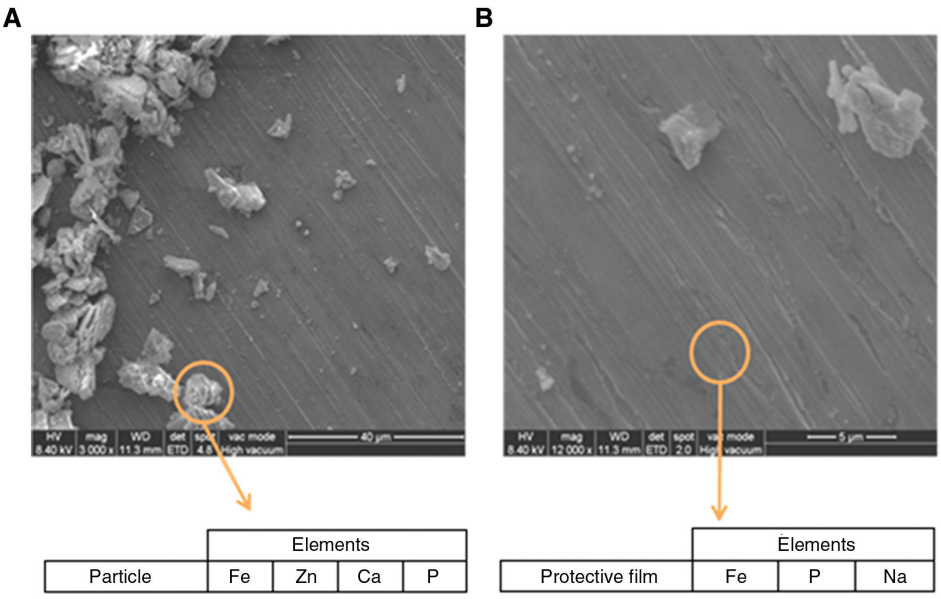

Figure 7: SEM micrograph and EDX of the protective film formed on the steel panels in contact with zinc phosphate suspensions in 0.05 M NaCl.

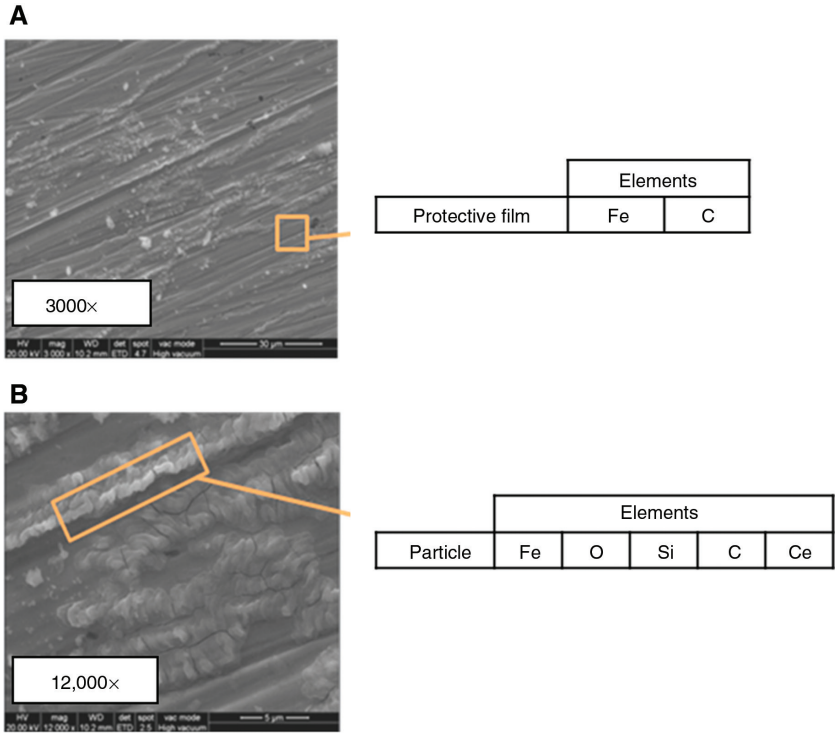

Figure 8: SEM micrograph and EDX of the protective film formed on the steel panels in contact with Z1Ce suspensions in 0.05 M NaCl.

on the painted surface. The evaluation was conducted by comparison with photographic standards. All paints blistered after 24 h of exposure in the humidity chamber except the control that showed no blisters (Table 8). The size and/or frequency of the blisters increased with time. Paints formulated with Z1Ce developed smaller blisters (qualification 6 after 168 h) compared with paints containing Z2Ce (qualified as 4 after 72 h). In every case, the blister density was medium. The development of blisters in the humidity chamber is expected when alkyd resins are used, but this feature does not constitute a problem because anticorrosion paints are top coated in service

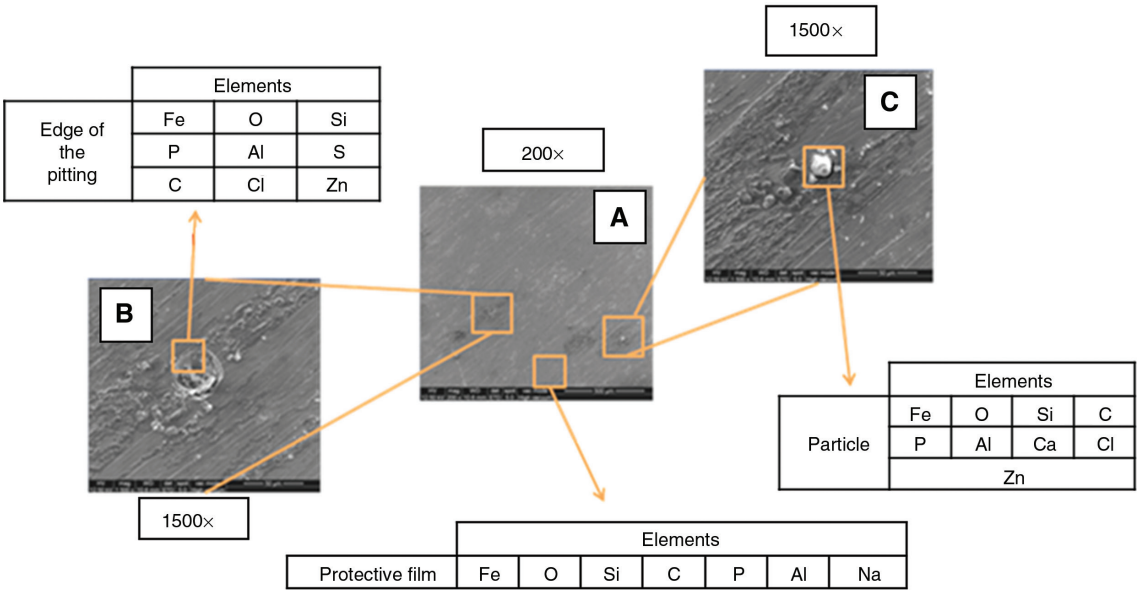

Figure 9: SEM micrograph and EDX of the protective film formed on the steel panels in contact with Z1Ce + PZ suspensions in 0.05 M NaCl.

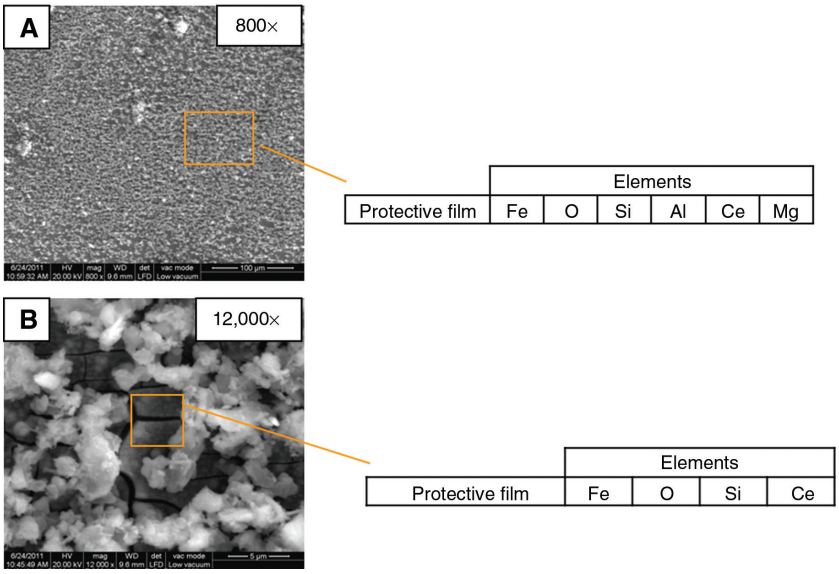

Figure 10: SEM micrograph and EDX of the protective film formed on the steel panels in contact with Z2Ce suspensions in 0.05 M NaCl.

conditions. After 168 h of exposure, panels were taken out the chamber due the onset of rusting after blistering.

3.2.2 Corrosion potential

At the beginning of the immersion time, the corrosion potential of painted panels was displaced towards more positive values except for paint 2A. This sample showed the worst anticorrosion behavior because it exhibited the most negative values from the beginning of the test (Figure 12). This more noticeable displacement to positive values for paints 1A, 1B, and 2B may be attributed to the presence, in the paint formulation, of Z1Ce or to the combination of the exchanged zeolites with PZ. However, as time elapsed, Ecorr values shifted towards more negative values, and after 2 weeks, most paints exhibited Ecorr values below –500 mV. The control paint had an almost constant value, close to –500 mV, along the test period.

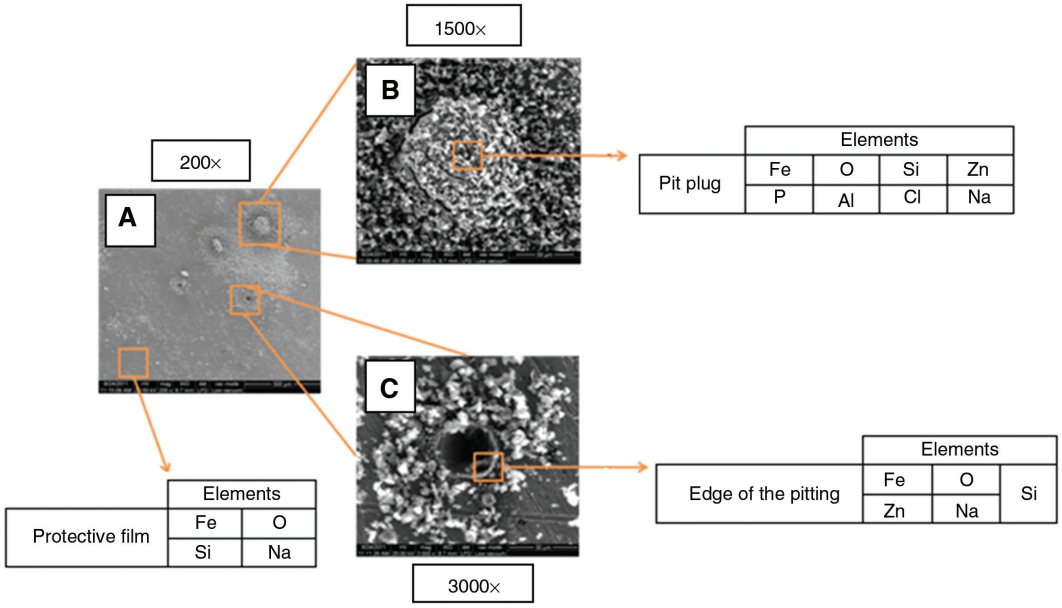

Figure 11: SEM micrograph and EDX analysis of the protective film formed on the steel panels in contact with Z2Ce + PZ suspensions in 0.05 M NaCl.

Table 7: Rusting degree (ASTM D 610) of painted panels in the salt spray chamber (ASTM B 117).

Paint	Time (h)				
	48	190	210	310	500
C	10	10	10	8G	8G
1A	10	10	9P	8P	8P
1B	10	10	8G	7G	5G
2A	8G	5G	–	–	–
2B	10	10	8G	7G	7G
Rusting degree	**10**	**9**	**8**	**7**	**6**	**5**
Rusted area (%)	0	0.01–0.03	0.03–0.1	0.1–0.3	0.3–1.0	1.0–3.0

Rust distribution types: S, spot; G, general; P, pinpoint.

Table 8: Blistering degree (ASTM D 744) of painted panels in the humidity chamber (ASTM D 2247).

Paint	Time (h)		
	24	72	168
C	10	10	10
1A	8 F	6 M	6 M
1B	8 F	6 M	6 M
2A	6 M	4 M	–
2B	8 M	6 M	–

Frequency	Dense (D)	Medium dense (MD)	Medium (M)	Few (F)
Size	10	8	6, 4	2
Comments	No blistering	Smaller size blister easily seen by unaided eye	Progressively larger sizes	

3.2.3 Electrochemical impedance spectroscopy

EIS is a valuable technique for acquiring information about processes taking place at the coating/substrate interface (Scully & Hensley, 1994; Grundmeier et al., 2000; Sorensen et al., 2009). The analysis of Bode's plots revealed a resistive-capacitive response of all tested paints; two of them are presented in Figure 13. However, the point of view adopted in this paper was that of Amirudin and Thierry (1995), i.e. the visual observation of the spectra could not indicate the exact number of time constants involved in the degradation of the organic coating subjected to a corrosive environment; in change, the number of these constants must be determined by data analysis by suitable procedures (Boukamp, 1989).

The equivalent circuit models used to fit experimental data were that shown in Figure 14, where Re is the electrolyte resistance, Rpo is the ionic resistance of the protective coating, Cc is the coating capacitance; Rt is the charge transfer resistance of the corrosion process, and Cdl is the double layer capacitance.

Distortions observed in the resistive-capacitive contributions indicate a deviation from the theoretical models due to either lateral penetration of the electrolyte at the

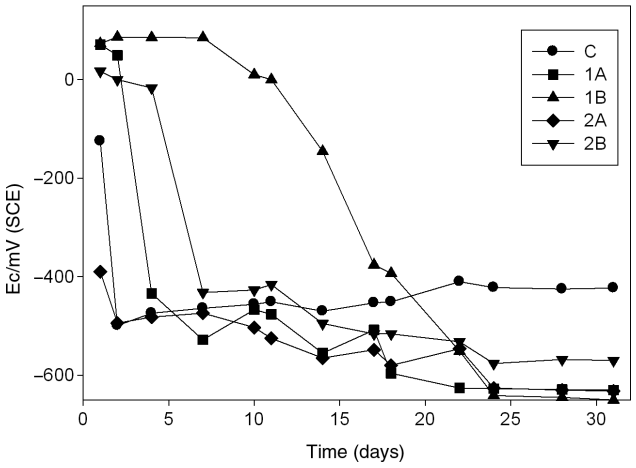

Figure 12: Time dependence of the corrosion potential (Ec) of painted panels in NaCl 0.5 M.

steel/paint interface (usually started at the base of intrinsic or artificial coating defects), underlying steel surface heterogeneity (topological, chemical composition, surface energy), or diffusional processes that could take place along the test. As all these factors cause the impedance/frequency relationship to be non-linear, they are taken into consideration by replacing the capacitive components (Ci) of the equivalent circuit transfer function by the corresponding constant phase element Qi (CPE), thus obtaining a better fit of data. The CPE is defined by the following equation:

$$Z = \frac{(j\omega)^{-n}}{Y_0}$$

where

Z = impedance of the CPE ($Z = Z' + Z''$) (Ω),
j = imaginary number ($j^2 = -1$),
ω = angular frequency (rad),
n = CPE power $n = \alpha/(\pi/2)$ (dimensionless),
α = constant phase angle of the CPE (rad), and
Y_0 = part of the CPE independent of the frequency (Ω^{-1}).

The accuracy of the fitting procedure was measured by the χ^2 parameter obtained from the difference between experimental and fitted data; the most probable circuit was selected providing that $\chi^2 < 10^{-4}$.

In the present work, the fitting process was mainly performed using the phase constant element Q_i instead of the dielectric capacitance C_i. However, this last parameter was used in the plots in order to facilitate results

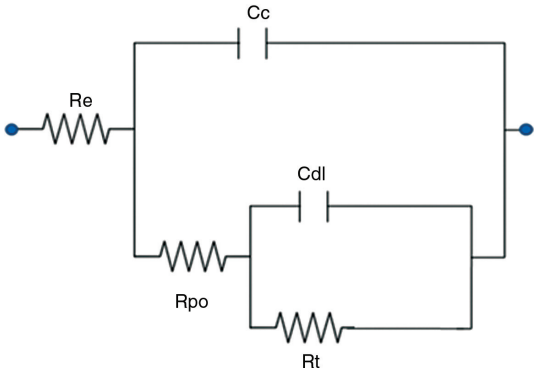

Figure 14: Equivalent circuit to interpret impedance data of a metal/paint-with-defects systems.

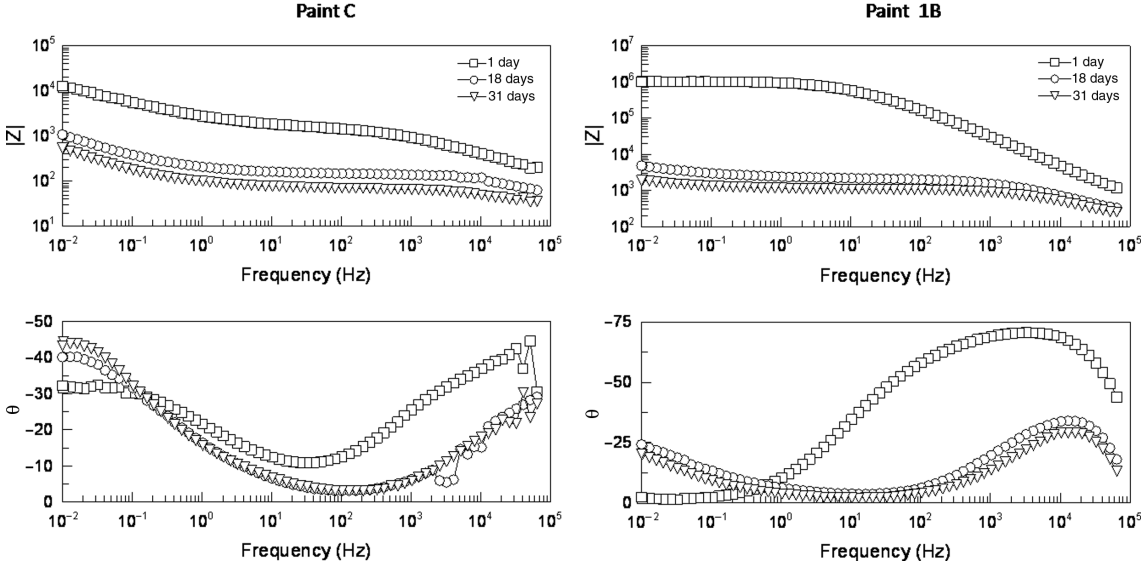

Figure 13: Bode's plots of selected painted panels in NaCl 0.5 M.

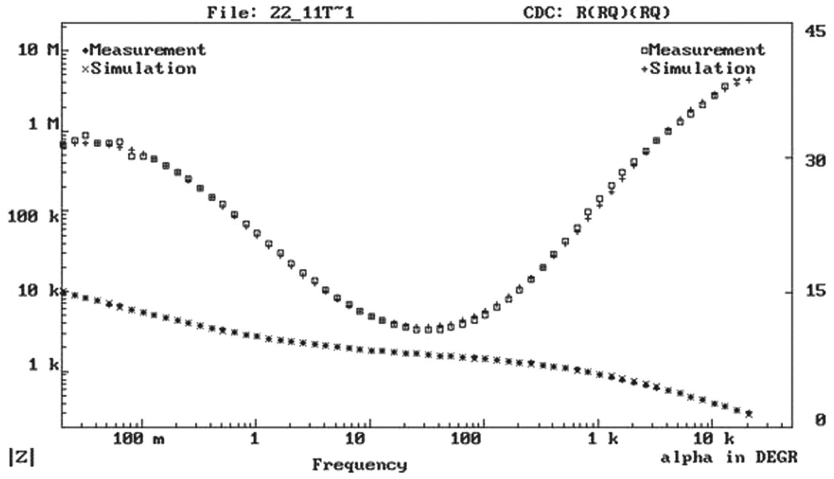

Figure 15: Fitting curve and experimental data of one of the painted panels.

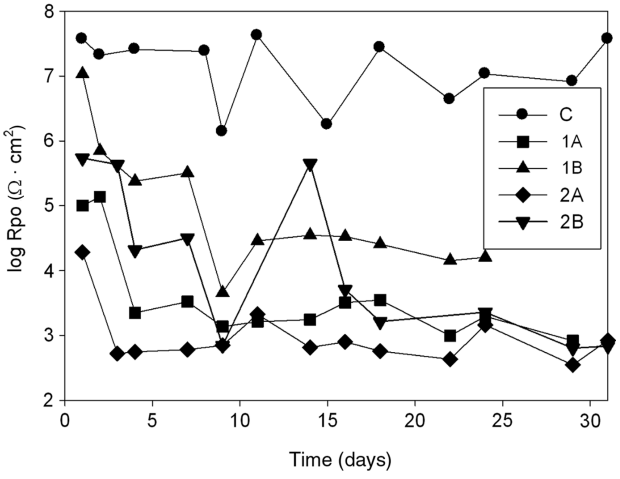

Figure 16: Time dependence of the electrolyte resistance (Rpo) of the painted panels systems in NaCl 0.5 M.

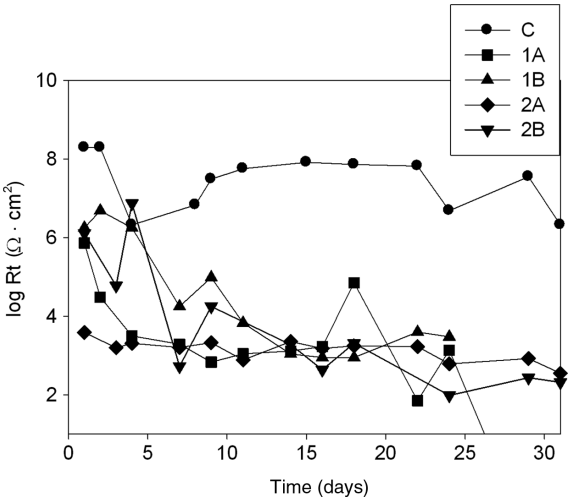

Figure 18: Time dependence of the charge transfer resistance (Rt) of the painted panels systems in NaCl 0.5 M.

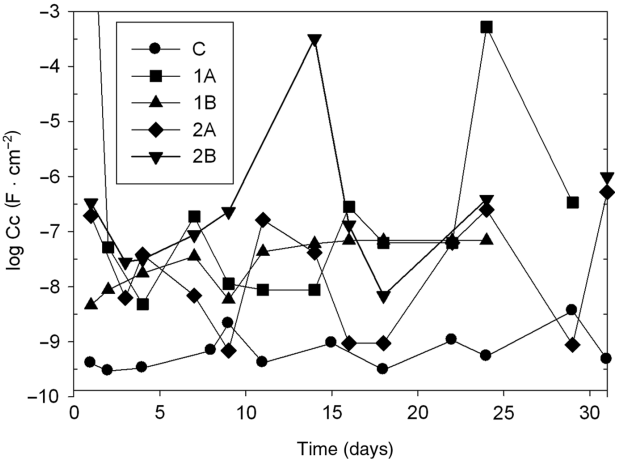

Figure 17: Time dependence of the capacitance (Cc) of the painted panels systems in NaCl 0.5 M.

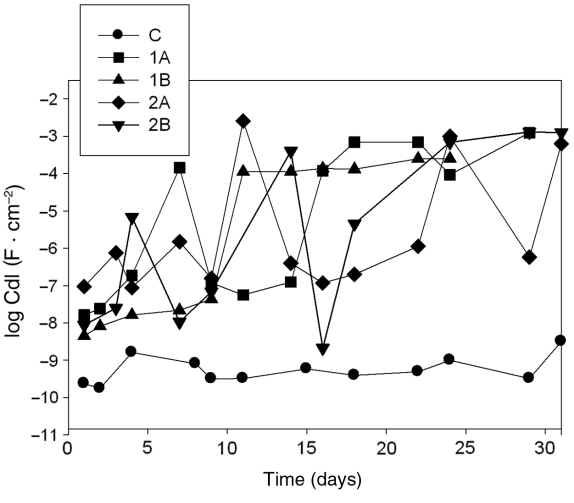

Figure 19: Time dependence of the of the double layer capacitance (Cdl) painted panels systems in NaCl 0.5 M.

visualization and interpretation. As an example, one of the fitted is presented in Figure 15.

The measured values of Rpo are shown in Figure 16. According to current literature (Grundmeier et al., 2000), the barrier effect is satisfactory when Rpo $\geq 10^8\ \Omega \cdot cm^2$ and a barrier residual effect is present if Rpo is between 10^6 and $10^8\ \Omega \cdot cm^2$. Paint C presented the highest values of Rpo, which oscillated around $10^7\ \Omega \cdot cm^2$. The observed oscillations in all the measurements may be attributed to temporary pore plugging by corrosion products. The incorporation of the modified zeolites to the paints reduced the barrier effect of the coatings almost from the beginning of the test. No significant barrier effect could be observed in the paints pigmented with the modified zeolites. The capacitance of the different coatings varied concomitantly with Rpo. Capacitance values in Figure 17 revealed that all coatings, except the control one, are not intact coatings because Cc was higher than $1 \times 10^{-9}\ F \cdot cm^{-2}$. In this sense, the control paint also showed signs of incipient deterioration.

The Rt values of the control paint C oscillated, as a trend, around 10^6 and $10^7\ \Omega \cdot cm^2$. Instead, during the first 11 days of immersion, Rt of all zeolite pigmented paints showed strong fluctuations between 10^4 and $10^7\ \Omega \cdot cm^2$ while the Rt of paint 2A maintained below $10^4\ \Omega \cdot cm^2$ (Figure 18). From this period on, Rt of all zeolite paints fluctuated between 10^3 and $10^4\ \Omega \cdot cm^2$. The protection afforded by the control paint relayed on its barrier properties in conjunction with the inhibitive action of the pigment, but in the other cases, the protection was derived from the inhibitive properties of the exchanged zeolites. This protection was enough to achieve a good behavior of the paints in the salt spray test.

The double layer capacitance values (Cdl) of the different coatings (Figure 19) showed an initial increase due to certain deterioration as water uptake by the film increased, followed by certain fluctuations of one or more orders of magnitude. The abnormal values observed for most paints ($Cdl > 10^{-6}\ F \cdot cm^{-2}$) suggested that Cdl may be regarded as a pseudo-capacitance more than a true one.

4 Conclusions

1. Zeolitic minerals can be used as carriers for passivating ions, like cerium, in anticorrosion paints.
2. The mineral containing more than 80% of mordenite resulted more adequate to develop a reservoir for cerium ions.
3. Zinc phosphate content can be totally or partially replaced by modified zeolites; this fact depends on characteristics of the zeolitic mineral. The zeolite constituted by mordenite and exchanged with Ce(III) may be used for full replacement of zinc phosphate. The other zeolite is useful for partial replacement of zinc phosphate.
4. The anticorrosion performance of the paints containing modified zeolites may be attributed to the inhibitive action of these pigments.

Acknowledgments: The authors are grateful to CONICET (Consejo Nacional de Investigaciones Científicas y Técnicas), UNLP (Universidad Nacional de La Plata), and CICPBA (Comisión de Investigaciones Científicas de la Provincia de Buenos Aires) for their sponsorship to do this research. The authors also thank Gonzalo Selmi for his technical support, to POLIDUR S.A. for providing the alkyd resin, and to Gerardo Rodriguez Fuentes for providing the zeolites to do this research work.

References

Abdullayev E, Price R, Shchukin D, Lvov Y. Halloysite tubes as nanocontainers for anticorrosion coating with benzotriazole. ACS Appl Mater Interfaces 2009; 1: 1437–1443.

Amirudin A, Thierry D. Application ef electrochemica impedance spectroscopy to study efficiency of anticorrosive pigment in epoxy-polyamide resin. Br Corros J 1995; 30: 128–134.

Armbruster T. In: Galarneau A, Di Renzo F, Fajula F, Vedrine J, editors. 13th International Zeolite Conference. Montpellier, France: Elsevier, 2001.

Ávila-Gonzalez C, Cruz-Silva R, Menchaca C, Sepulveda-Guzman S, Uruchurtu J. Use of silica tubes as nanocontainers for corrosion inhibitor storage. J Nanotechnol 2011; 2011: 461313–461322.

Baghdachi J. Smart coatings. In: Report 2004, Buenos Aires, 2004.

Barraclough J, Harrison JB. New leadless anti-corrosive primers. J Oil Col Chem Assoc 1965; 48: 341–355.

Behrsing T, Deacon GB, Junk PC. The chemistry of rare earth metals, compounds, and corrosion inhibitors. In: Forsyth M, Hinton BRW, editors. Rare earth-based corrosion inhibitors. UK: Woodhead Publishing, 2014: 1–37.

Bethencourt M, Botana FJ, Calvino JJ, Marcos M, Rodríguez-Chacón MA. Lanthanide compounds as environmentally-friendly corrosion inhibitors of aluminium alloys: a review. Corros Sci 1998; 40: 1803–1819.

Bhanvase BA, Patel MA, Sonawane SH. Kinetic properties of layer-by-layer assembled cerium zinc molybdate nanocontainers during corrosion inhibition. Corros Sci 2014; 88: 170–177.

Bittner A. Advanced phosphate anticorrosive pigments for compliant primers. J Coat Technol 1989; 61: 111–118.

Borisova D, Möhwald H, Shchukin DG. Influence of embedded nanocontainers on the efficiency of active anticorrosive coatings for aluminum alloys part ii: influence of nanocontainer position. ACS Appl Mater Interfaces 2013; 5: 80–87.

Boukamp BA. Equivalent circuit. Report CT88/265/128, CT89/214/128, 1989.

Carneiro J, Caetano AF, Kuznetsova A, Maia F, Salak AN, Tedim J, Scharnagl N, Zheludkevich ML, Ferreira MGS. Polyelectrolyte-modified layered double hydroxide nanocontainers as vehicles for combined inhibitors. RSC Adv 2015; 5: 39916–39929.

Cecílio P, Duarte RG, Simões AM, Ferreira MGS, Montemor MF. The effect of cerium nitrate on the corrosion behavior of electrogalvanized steel substrates, evaluated by XPS and SVET. In: Fedrizzi L, Terryn H, Simões AM, editors. Innovative pre-treatment techniques to prevent corrosion of metallic surfaces. England: Woodhead Publishing, 2007: 110–118.

Columbié Pineda R, Rodriguez Fuentes G, Victorero Rodriguez A, Prieto Valdés JJ. Utilizacion de zeolitas modificadas en la obtencion de recubrimientos de zeosil. In: Zeolites '91: Ocurrencia, Propiedades y usos de las zeolitas naturales, La Habana, Cuba, 1991.

Chen T, Fu J. An intelligent anticorrosion coating based on pH-responsive supramolecular nanocontainers. Nanotechnology 2012; 23: Article 505705.

del Amo B, Romagnoli R, Vetere VF. Study of the anticorrosive properties of zinc phospahte and zinc molybdophosphate in alkyd paints. Corros Rev 1996; 14: 121–133.

del Amo B, Deyá M, Mercader R, Salva P, Sives F. Extracción de hierro de rocas zeolíticas. In: XI Jornadas de Jóvenes Investigadores de AUGM y 1° Encuentro de Jóvenes Investigadores de la UNLP, La Plata, Bs. As., Argentina, 2003.

Deyá C, Blustein G, del Amo B, Romagnoli R. Evaluation of eco-friendly anticorrosive pigments for paints in service conditions. Progr Org Coat 2010; 69: 1–6.

Deyá C, del Amo B, Spinelli E, Romagnoli E. The assessment of a smart anticorrosive coating by the electrochemical noise technique. Progress in Organic Coatings 2013; 76: 525–532.

DHHS-NIOSH. Registry of toxic effects of chemical substances, ed., 1986.

Dias SAS, Lamaka SV, Nogueira CA, Diamantino TC, Ferreira MGS. Sol–gel coatings modified with zeolite fillers for active corrosion protection of AA2024. Corros Sci 2012; 62: 153–162.

Eunjoo K, Nam-Kyun K, Jihoon S, Young-Wun K. Polyurethane microcapsules for self-healing paint coatings. RSC Adv 2014; 4: 16214–16233.

Falcón JM, Sawczen T, Vieira Aoki I. Dodecylamine-loaded halloysite nanocontainers for active anticorrosion coatings. Frontiers Mater 2015; 2: Article 69.

Feng YC, Cheng YF. Fabrication of Halloysite nanocontainers and their compatibility with epoxy coating for anti-corrosion performance. Corros Eng Sci Technol 2016; 51: 489–497.

Ferrazzini JC. Molecular sieve powders for paints and sealants. Paint Resin 1986; 56: 33.

Fragata FdL, Dopico JE. Anticorrosive behavior of zinc phosphate in alkyd and epoxy binders. J Oil Col Chem Assoc 1991; 74: 92–97.

Gerhard A, Bittner A. Second generation phosphate anticorrosive pigments. Formulating rules for full replacement of new anticorrosive pigments. J Coat Technol 1986; 58: 59–65.

Gottesfeld P. Time to ban lead in industrial paints and coatings. Frontiers Public Health 2015; 3: Article 144.

Granizo N, Vega JM, Díaz I, Chico B, de la Fuente D, Morzillo M. Paint systems formulated with ion-exchange pigments applied on carbon steel: effect of surface preparation. Prog Org Coat 2011; 70: 394–400.

Greenwood NN, Earnshaw A. Chemistry of the elements, 1st ed., Oxford, England: Pergamon, 1984.

Grundmeier G, Schmidt W, Stratmann M. Corrosion protection by organic coatings: electrochemical mechanism and novel methods of investigation. Electrochim Acta 2000; 45: 2515–2533.

Haley TJ. Pharmacology and toxicology of the rare earth elements. J Pharm Sci 1965; 54: 663–670.

Hang TTX, Truc TA, Duong NT, Pébère N, Olivier M-G. Layered double hydroxides as containers of inhibitors in organic coatings for corrosion protection of carbon steel. Prog Org Coat 2012; 74: 343–348.

Hao Y, Liu F, Han E-H, Anjum S, Guobao X. The mechanism of inhibition by zinc phosphate in an epoxy coating. Corros Sci 2013; 69: 77–86.

Jaškova V, Kalendová A. Anticorrosive coatings containing modified phosphates. Prog Org Coat 2012; 75: 328–334.

Kartsonakis IA, Koumoulos EP, Balaskas AC, Pappas GS, Charitidis CA, Kordas GC. Hybrid organic–inorganic multilayer coatings including nanocontainers for corrosion protection of metal alloys. Corros Sci 2012; 57: 56–66.

Kesavan D, Gopiraman M, Sulochana N. Green inhibitors for corrosion of metals: a review. Che Sci Rev Lett 2012; 1: 1–8.

Klaassen CD. Casarett and Doull's Toxicology. The basic science of poisons, 5th ed., USA: The McGraw-Hill Companies, Inc., 1999.

Kozlowski W, Flis J. An ellipsometric phosphate study of the effect of anions in borate solution on anodic films grown on iron. Corros Sci 1991; 32: 861–875.

Lakshmi RV, Aruna ST, Anandana C, Bera P, Sampath S. EIS and XPS studies on the self-healing properties of Ce-modified silica-alumina hybrid coatings: evidence for Ce(III) migration. Surf Coat Technol 2017; 309: 363–370.

Lenz DM, Delamar M, Ferreira CA. Improvement of the anticorrosion properties of polypyrrole by zinc phosphate pigment incorporation. Prog Org Coat 2007; 58: 64–69.

Liu M, Guo B, Lei Y, Du M, Jia D. Benzothiazole sulfide compatibilized polypropylene/halloysite nanotubes composites. Appl Surface Sci 2009; 255: 4961–4969.

Lu YC, Ives MB. The improvement of the localized corrosion resistance of stainless steel by cerium. Corros Sci 1993; 34: 1773–1785.

Meyer G. Uber Zinkphosphat und Bariumchromat als moderne Korrosionsinhibitoren. Farbe u. Lack 1963; 7: 528–532.

Ming DW, Allen ER. Recent advances in the United States in the use of natural zeolites in plant growth. In: International Conference on the Occurrence, Properties and Utilization of Natural Zeolites (5th: 1997: Naples, Italy), Napoly, Italy, 1997.

Montemor MF, Snihirova DV, Taryba MG, Lamaka SV, Kartsonakis IA, Balaskas AC, Kordas GC, Tedim J, Kuznetsova A, Zheludkevich ML, Ferreira MGS. Evaluation of self-healing ability in protective coatings modified with combinations of layered double hydroxides and cerium molibdate nanocontainers filled with corrosion inhibitors. Electrochim Acta 2012; 60: 31–40.

Naderi R, Attar MM. Electrochemical study of protective behavior of organic coating pigmented with zinc aluminum polyphosphate as a modified zinc phosphate at different pigment volume concentrations. Prog Org Coat 2009; 66: 314–320.

Naderi R, Mahdavian M, Darvish A. Electrochemical examining behavior of epoxy coating incorporating zinc-free phosphate-based anticorrosion pigment. Prog Org Coat 2013; 76: 302–306.

Odum EP. Ecología, 3rd ed., USA: The McGraw-Hill Companies, Inc., 1972.

Romagnoli R, Vetere FV. Non pollutant corrosion inhibitive pigments: zinc phosphate, a review. Corros Rev 1995a; 13: 45–64.
Romagnoli R, Vetere FV. Heterogeneous reaction between steel and zinc phsophate. Corrosion 1995b; 51: 116–123.
Romagnoli R, del Amo B, Vetere VF, Vèleva L. High performance anticorrosive epoxy paints pigmented with zinc molybdenum phosphate. Surface Coat Inte 2000; 83: 27–31.
Scully JR, Hensley ST. Lifetime prediction for organic coatings on steel and a magnesium alloy using electrochemical impedance methods. Corrosion 1994; 50: 705–716.
Shchukin D, Möhwald H. Self-repairing coatings containing active nanoreservoirs. Small 2007; 3: 926–943.
Shkirskiy V, Keil P, Hintze-Bruening H, Leroux F, Vialat P, Lefèvre G, Ogle K, Volovitch P. Factors affecting $MoO4^{2-}$ inhibitor release from Zn_2Al based layered double hydroxide and their implication in protecting hot dip galvanized steel by means of organic coatings. ACS Appl Mater Interfaces 2015; 7: 25180–25192.
Sorensen SK, Dam-Johansen K, Weinell C. Anticorrosive coatings: a review. J Coat Technol Res 2009; 6: 135–176.
Szabó T, Molnár-Nagy L, Bognár J, Nyikos L, Telegdi J. Self-healing microcapsules and slow release microspheres in paints. Prog Org Coat 2011; 72: 52–57.
Szklarska-Smialowska Z, Mankowsky J. Cathodic inhibition of the corrosion of mild steel in phosphate, tungstate, arsenate and silicate solutions containing Ca^{2+} ions. Brit Corr J 1969; 4: 271–275.
Tedim J, Zheludkevich ML, Salak AN, Lisenkov A, Ferreira MGS. Nanostructured LDH-container layer with active protection functionality. J Mater Chem 2011; 21: 15464–15470.
Torii K. Utilization of natural zeolites in Japan, In: Sand LB, Mumpton FA, editors. Natural zeolites: occurrence, properties and uses. Oxford, England: Pergamon, 1978: 441–450.
Welcher F. Organic analytical reagents, ed., New York, USA: D. Van Nostrand Company, Inc., 1948.
Xiangyu L, Yu Z, Xuhui Z, Yuming T. The influence of aluminum tri-polyphosphate on the protective behavior of Mg-rich epoxy coating on AZ91D magnesium alloy. Electrochim Acta 2013; 93: 53–64.
Yan S, Heb W, Sun C, Zhang X, Zhao H, Li Z, Zhou W, Tian X, Sun X, Han X. The biomimetic synthesis of zinc phosphate nanoparticles. Dyes Pigments 2009; 80: 254–258.
Yan H, Wang J, Zhang Y, Hu W. Preparation and inhibition properties of molybdate intercalated ZnAlCe layered double hydroxide. J Alloys Compd 2016; 678: 171–178.
Yuhua D, Liqin M, Qiong Z. Effect of the incorporation of montmorillonite-layered double hydroxide nanoclays on the corrosion protection of epoxy coatings. J Coat Technol Res 2013; 10: 909–921.
Zalba P. Zeolitas, el mineral del siglo. Ciencia e Investigación 1996; April: 40–51.
Zarras P, Stenger-Smith JD. Smart inorganic and organic pretreatment coatings for the inhibition of corrosion of metals/alloys. In: Tiwari A, Rawlings J, Hihara LH, editors. Intelligent coatings for corrosion control. USA: Elsevier, 2015: 59–79.
Zheludkevich ML, Shchukin DG, Yasakau KA, Möhwald H, Ferreira MGS. Anticorrosion coatings with self-healing effect based on nanocontainers impregnated with corrosion inhibitor. Chem Mater 2007; 19: 402–411.
Zheludkevich ML, Poznyak SK, Rodrigues LM, Raps D, Hack T, Dick LF, Nunes T, Ferreira MGS. Active protection coatings with layered double hydroxide nanocontainers of corrosion inhibitor. Corros Sci 2010; 52: 602–611.
Zheludkevich M, Tedim J, Ferreira M. “Smart” coatings for active corrosion protection based on multi-functional micro and nanocontainers. Electrochim Acta 2012; 82: 314–323.
Zhu Y, Zhuang J, Yu Y, Zeng X. Research on anti-corrosion property of rare earth inhibitor for X70 steel. J Rare Earths 2013; 31: 734–740.